

Silver L_1 , L_2 and L_3 cross-sections for ionization and x-ray production by electron impact

This content has been downloaded from IOPscience. Please scroll down to see the full text.

2014 J. Phys. B: At. Mol. Opt. Phys. 47 215006

(<http://iopscience.iop.org/0953-4075/47/21/215006>)

View [the table of contents for this issue](#), or go to the [journal homepage](#) for more

Download details:

This content was downloaded by: gcas_1

IP Address: 200.16.16.13

This content was downloaded on 24/10/2014 at 10:28

Please note that [terms and conditions apply](#).

Silver L_1 , L_2 and L_3 cross-sections for ionization and x-ray production by electron impact

A Sepúlveda^{1,2}, A P Bertol³, M A Z Vasconcelos³, J Trincavelli^{1,2},
R Hinrichs⁴ and G Castellano^{1,2}

¹FaMAF, Universidad Nacional de Córdoba, M. Allende s/n, Ciudad Universitaria (5000), Córdoba, Argentina

²IFEG, CONICET, Argentina

³Instituto de Física, Universidade Federal de Rio Grande do Sul, Porto Alegre, Rio Grande do Sul, Brazil

⁴Instituto de Geociências, Universidade Federal de Rio Grande do Sul, Porto Alegre, Rio Grande do Sul, Brazil

E-mail: gcas@famaf.unc.edu.ar

Received 17 April 2014, revised 5 September 2014

Accepted for publication 9 September 2014

Published 23 October 2014

Abstract

The experimental determination of ionization cross-sections and total x-ray production cross-sections under electron impact is carried out for the three silver L-subshells. The very complex spectral structure involving several satellite bands was previously investigated by analyzing wavelength-dispersive spectra acquired in an electron microprobe. In this work, careful spectral processing is carried out by means of the POEMA software developed previously, considering the spectral energy intervals which include the main Ag-L emissions. The resulting ionization cross-sections are compared with analytical models based on distorted wave Born approximation calculations, the experimental determinations of the present work being underestimated by these predictions. To the best of the authors' knowledge, this is the first time these magnitudes are reported in the literature in this energy range. The total L-shell x-ray production cross-sections are also compared with the only previous experimental data found, obtained with different experimental settings.

Keywords: inner-shell ionization, x-ray emission, spectral processing

1. Introduction

Ionization cross-sections represent the probability for a specific interaction between a particular projectile and a target atom, after which the latter is left ionized. Atom relaxation after this event can result in Auger transitions or in the emission of characteristic x-rays. The probability for the whole process of ionization and x-ray emission is called x-ray production cross-section (normalized for the number of target atoms per unit area and per incident particle); it may be computed for each of the subshells constituting an atomic shell or as a whole phenomenon. An inherent basic interest surrounds the adequate knowledge of these cross-sections, since it permits us to validate different theoretical models in the frame of atomic physics. On the other hand, the

appropriate experimental determination of these parameters is relevant for many applications involving characteristic x-ray emission or electron stopping power in materials [1–3].

Several spectrochemical analytical techniques require a precise understanding of the ionization cross-sections for the elements constituting the target materials, since the uncertainties in these parameters are straightforwardly transferred to the elemental concentrations assessed. This becomes particularly important in the case of absolute (standardless) quantification methods [4].

A number of theoretical models for the ionization cross-sections have been developed, based on the plane wave Born approximation [5, 6], distorted-wave calculations (DWBA) [7–10], binary-encounter Bethe model [11, 12], etc. However, experimental determinations are rather unusual, although they

are quite necessary for the proper validation of these approaches. This scarcity of experimental data is mainly due to the difficulties inherent to the experimental determinations and the inconveniences in data processing. In particular, no experimental data are found in the literature for separate L-subshell ionization cross-sections in the energy range studied; only the global x-ray production cross-section has been reported [13].

In the thin sample approach, characteristic peak intensities are proportionally related to ionization cross-sections (4); however, the fabrication of thin samples and the determination of their thickness imply dealing with important difficulties [14, 15]. In order to overcome some of these difficulties, film deposits on top of low atomic number bulk substrates are often used [16, 17]. In contrast, the method proposed by An *et al* for bulk samples [18, 19] bears three major drawbacks: on the one hand, linear trajectories are assumed within the sample, disregarding electron straggling, which may result in strong overestimations in the self-absorption correction factors; on the other hand, a numerical differentiation is required to derive the cross-sections from the experimental characteristic intensities as a function of the incident energy E_o , which usually implies extra error sources; finally, backscattering losses are not taken into account, which implies different corrections for the different incident energies, generating artificial biases for the final cross-section values.

In this work, the experimental determination of L-subshell ionization cross-sections for silver has been faced using a thin-film on top of a bulk substrate, which required the fabrication of metal deposits upon carbon substrates, as detailed in section 2. In order to take advantage of this approach, it is convenient to recall the definitions of effective ionization cross-sections. Once an ionization has been produced in a multiple atomic shell, primary vacancies are rearranged through Coster–Kronig transitions [20], which modify the characteristic photon emission, giving rise to the following effective ionization cross-sections

$$\begin{aligned}\sigma_{L_1}^{\text{eff}} &= \sigma_{L_1} \\ \sigma_{L_2}^{\text{eff}} &= \sigma_{L_2} + f_{12} \sigma_{L_1} \\ \sigma_{L_3}^{\text{eff}} &= \sigma_{L_3} + f_{23} \sigma_{L_2} + (f_{13} + f_{12} f_{23}) \sigma_{L_1},\end{aligned}\quad (1)$$

where σ_{L_1} , σ_{L_2} , σ_{L_3} are the subshell ionization cross-sections by electron impact and f_{12} , f_{23} , f_{13} are the Coster–Kronig transition probabilities. With these definitions, it is useful to introduce the total x-ray production cross-section for the L-shell as

$$\sigma_{L_x} = \omega_1 \sigma_{L_1}^{\text{eff}} + \omega_2 \sigma_{L_2}^{\text{eff}} + \omega_3 \sigma_{L_3}^{\text{eff}},\quad (2)$$

where ω_1 , ω_2 , ω_3 are the fluorescence yields for the corresponding L-subshell. This magnitude is often used in the literature [8, 21, 22] and is proportional to the probability of emitting an L characteristic x-ray photon, regardless of which other shells are involved in the decay.

Cross-sections were obtained from spectra acquired in an energy-dispersive spectrometer (EDS). To this aim, the

parameter refinement program POEMA was used [23, 24], applying it to different data sets generated through electron impact at different incident energies. In the spectral processing routine, several instrumental parameters are involved, like the detector intrinsic efficiency and the solid angle subtended by it, as well as atomic parameters such as radiative transition rates, characteristic emission energies, fluorescence yields, and Coster–Kronig transition probabilities. The values obtained are finally compared with experimental data from the literature as well as with DWBA predictions.

2. Experimental setup

An Ag film was deposited on vitreous carbon planchets (Ted Pella) by magnetron sputtering (AJA International ATC ORION 8 UHV), using an ultrapure (99.999%) Ag target. Carbon was chosen as the substrate in order to take advantage of its low backscattering yield. The areal density $(Nt)_{\text{film}}$ was determined by Rutherford backscattering spectrometry (RBS), using 1 MeV alpha-particles in an ion accelerator (High Voltage Engineering, Tandetron 3MV), and the SIMNRA [25] software was used to fit the experimental results. The areal density obtained for the Ag film was $(49.00 \pm 0.26) \times 10^{15}$ at/cm². After the treatment of the RBS spectra, a very thin oxidation layer was found, amounting to $(6.5 \pm 0.1) \times 10^{15}$ oxygen atoms per cm².

The electron gun of a multibeam SEM-FIB (JEOL JIB-4500) was used to excite the spectra from the Ag thin sample, which were acquired using an EDS with a silicon drift detector (SDD Thermo Scientific Ultradry) with a 150 eV resolution (FWHM) for Fe-K α . According to the supplier, this detector has an effective area of 10 mm², a 300 nm polymer window, a 30 nm aluminum ohmic contact, and a 10 nm dead layer. The detector efficiency is reduced by a factor of 0.77 due to the shadowing of the grid that supports the ultrathin window. Measurements were performed with a 35° takeoff angle (18 mm working distance), 300 s average live time, a sample-detector distance of 58 mm, and probe currents around 2 nA, which were measured with a Faraday cup. The solid angle subtended by the detector active surface is $(2.01 \pm 0.12) \times 10^{-3}$ sr (see subsection 3.2).

The magnetron sputterer used is known to produce samples of very regular thickness over areas as large as 100 cm². The reproducibility of x-ray spectra taken at different positions in such samples has been repeatedly demonstrated in former measurements; for this reason, in this work single spectra were acquired for 6, 7, 8, 9, 10, 12, 15, 20, and 25 keV incident energy over a scanned area of 10×10 μm^2 .

Since the EDS spectrometer inhibits the discrimination of the many different Ag-L emission lines, the values for the characteristic energies and for the transition rates were determined from previous fittings to spectra acquired when irradiating a bulk Ag standard using a wavelength dispersive spectrometer (WDS), for which the energy resolution is much better [26]. For thin targets, instead, a very weak signal is emitted, which implies that statistically acceptable spectra in a

WDS would require either too high beam currents, which might induce sample damage, or impracticably long acquisition times. For this reason, EDS spectra were acquired by means of an SDD whose absolute efficiency is very high.

3. Methodology

3.1. Spectral processing

The POEMA program used to fit each spectrum has been carefully described previously [17, 23, 24, 27]. Starting from initial estimates for the different parameters involved in the spectrum description, it is possible to improve the initial prediction through an iterative procedure which minimizes the quadratic differences between the experimental and the predicted spectra. The expression included in the program POEMA for the estimated number of photons I'_i in the energy interval $[E_i, E_i + \Delta E]$ associated with the i th channel is

$$I'_i = \left[\alpha_B B(Z, E_o, E_i) + \sum_{j,k} P_{j,k} H_{j,k}(E_i) + P_{\text{ox}} H_{\text{ox}}(E_i) + P_{\text{subs}} H_{\text{subs}}(E_i) \right] \Delta E, \quad (3)$$

where the bremsstrahlung emission B is an analytical function of the atomic number Z , the incident energy E_o , and the photon energy E_i [28], α_B is a scaling factor for this continuum, P and H are, respectively, the characteristic peak intensity and a peak-shaping function [29] for the k line of element j in the film, and the same stands for the oxide (ox) and the substrate (subs).

For a film of areal density $(Nt)_{\text{film}}$ deposited on a carbon substrate, irradiated with N_e incident electrons, $P_{j,k}$ can be written as [27]

$$P_{j,k} = N_e (Nt)_{\text{film}} \Gamma_{j,k} \omega_i \sigma_{L_i}^{\text{eff}} \varepsilon \frac{\Delta\Omega}{4\pi} \Phi_{\text{oc}}, \quad (4)$$

where $\Gamma_{j,k}$ is the relative transition probability for the k line of element j , and ε and $\Delta\Omega$ are the intrinsic efficiency at the considered energy and the solid angle subtended by the detector, respectively. The surface ionization Φ_{oc} includes the effect that electrons backscattered in the substrate ionize the film [17]. The global parameters that can be refined by POEMA are the scale factor involved in the bremsstrahlung prediction (assessed for the carbon substrate, since the film contribution is negligible), the spectrometer gain and zero, the parameters related to peak widths, and the spontaneous oxide layer thickness. Individual peak parameters can be also optimized by the program, such as asymmetry coefficients, elemental concentrations, and relative transition probabilities.

3.2. Solid angle

To determine the solid angle subtended by the x-ray detector, the bremsstrahlung generated between 3–6 keV by a carbon substrate when irradiated with 15-keV electrons was simulated with the PENCYL program of the PENELOPE software [30]. On the other hand, an x-ray spectrum

corresponding to the same conditions was measured with the EDS, whose solid angle is to be obtained. Bearing in mind that in the considered energy range the intrinsic efficiency of the detector is almost constant, the solid angle can be determined from the ratio between the measured and simulated bremsstrahlung. The solid angle obtained was $(2.01 \pm 0.12) \times 10^{-3}$ sr [17].

3.3. Ionization cross-section

With the aim of determining experimental values σ_{L_i} for each L_i -subshell ionization cross-section, it is useful to define

$$\sigma_{L_i} = \alpha_{L_i} \sigma_{L_i}^{\text{th}}, \quad (5)$$

where α_{L_i} is introduced as a correction factor for the theoretical prediction $\sigma_{L_i}^{\text{th}}$ used by the program [31]. The software POEMA permits us to involve these as fitting parameters, therefore allowing us to determine σ_{L_i} for all subshells.

As mentioned above, since EDS spectrometers do not bear appropriate energy resolution so as to discriminate all L-emissions, values for transition rates and emission energies were taken from previous fittings to WDS spectra [26]. Maintaining these values fixed, EDS spectra induced by electron impact were fitted, for incident energies of 6, 7, 8, 9, 10, 12, 15, 20, and 25 keV. The fitting parameters involved in these refinements are the detector gain and zero, the bremsstrahlung scale α_B , and the α_{L_i} correction factors. For the calibration process, the most intense emission lines from Ag were considered; once this calibration was completed, the Duane–Hunt limit was verified for each spectrum with the aim of validating the nominal incident energies. It is important to stress that the σ_{L_i} values obtained by this method are independent of how appropriate the model chosen for $\sigma_{L_i}^{\text{th}}$ is, since only the product $\alpha_{L_i} \sigma_{L_i}^{\text{th}}$ is relevant.

3.4. Validation of the thin-film approach (by Monte Carlo simulation)

The emitted characteristic intensity should be proportional to the sample thickness as long as the thin-film hypothesis is fulfilled; i.e., (4) is valid only if the beam electrons as well as those backscattered in the carbon substrate undergo at most only one interaction. With the aim of checking the validity of this hypothesis, a set of Monte Carlo simulations was carried out for each beam energy, target thickness ranging from 1–20 nm.

The PENELOPE routine package was used to this aim [30] by modifying the PENCYL main program provided in the 2011 distribution, so that the emitted x-rays taken into account correspond to the 35° takeoff angle of the experimental mount used in the present measurements. For each of the incident energies pointed in the previous section, x-ray spectra were therefore simulated, varying the silver layer thickness from 1–20 nm. Figure 1 displays an example involving the results obtained for $L_3M_5 + L_3M_4$ net intensities as a function of the Ag layer thickness for 8 keV beam electrons. In this case, the thin film regime is valid up

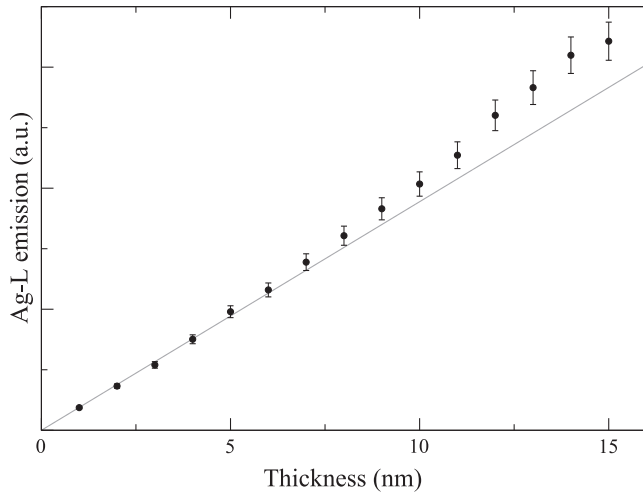


Figure 1. Monte Carlo simulations of characteristic Ag-L emission from target thickness ranging from 1–20 nm for 8 keV beam electrons: ● simulated intensity;—linear fit for data in the thin film regime. Error bars correspond to statistical uncertainties (three standard deviations).

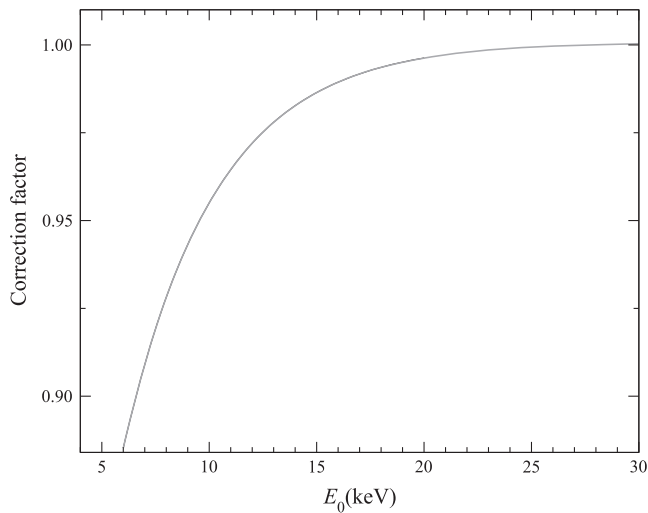


Figure 2. Correction function, corresponding to the 9.6 nm sample used here, to account for the deviations from the thin film regime.

to around 6 nm, where a linear fit was carried out. For the cases where the thin film hypothesis is not fulfilled, a factor can be obtained from this fitting procedure to correct the ionization cross-sections derived from the experimental intensities.

For the sample thickness involved here (9.6 nm), a correction factor was obtained for each energy studied. For this thickness, the CPU time required for the simulations amounted up to several days to reduce the statistical uncertainties below 5%. The correction factors obtained were fitted as a function of the beam energy in order to smooth their inherent fluctuations. Figure 2 shows this fitted function, which was used to account for the deviations from the thin film regime.

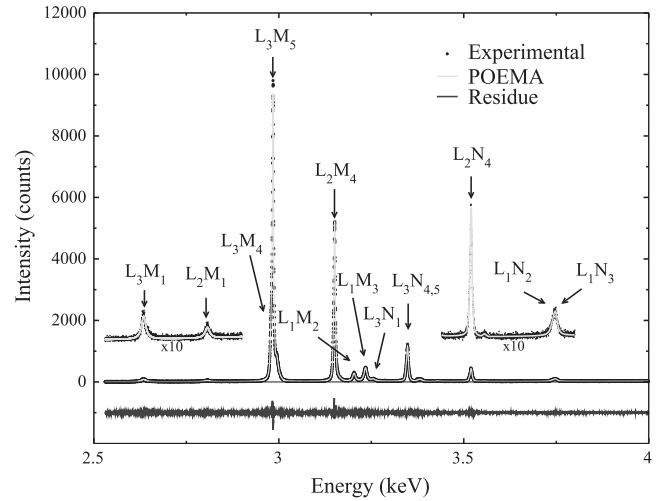


Figure 3. Ag L spectrum acquired with a WDS spectrometer for 20 keV incident energy.

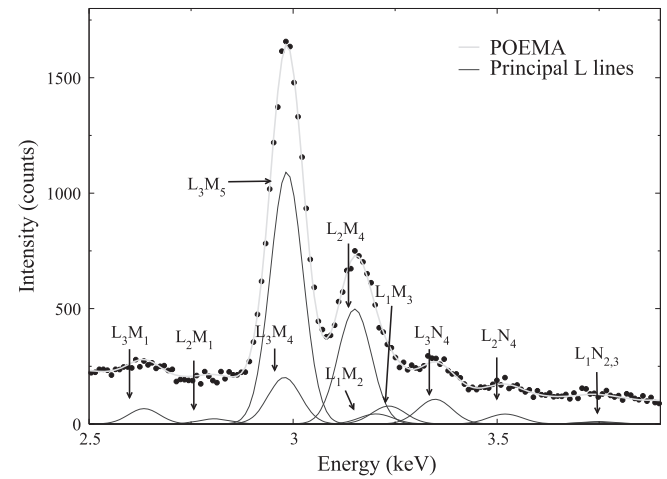


Figure 4. Ag L spectrum acquired with an EDS spectrometer for 9 keV incident energy.

4. Results and discussion

Figure 3 shows the region of interest of the WDS Ag-L spectrum generated by 20 keV impinging electrons [26], in which the main diagram lines have been labeled. Since an optimum agreement between the spectrum predicted by POEMA and the experimental data was achieved, the values obtained through this fitting process for emission energies and transition rates have been taken as a reference for the refinements carried out along the present work.

Due to the fact that in an EDS detector peak-to-background ratios are quite smaller than those obtained in a WDS, the weakest emissions cannot be determined for the case of 20 keV incident energy. However, as the incident energy is reduced, the probability for producing ionizations in the L-shell increases; figure 4 displays an EDS spectrum for 9 keV electrons, labeling the different emissions as identified in the WDS spectrum. The inclusion of these lines allows us to maintain the emission energies and the relative intensities fixed along the refinement process carried out in this work.

Table 1. Fluorescence yields and Coster–Kronig probabilities used in the assessments: (a) Perkins *et al* [34]; (b) Campbell [33].

	Fluorescence yields			Coster–Kronig probabilities		
	ω_1	ω_2	ω_3	f_{12}	f_{13}	f_{23}
a	0.014879	0.054703	0.057018	0.09211	0.6644	0.1604
b	0.016	0.051	0.052	0.068	0.57	0.141

This becomes particularly important, since disregarding these emissions that are difficult to determine in the measured EDS spectra, may considerably modify the cross-sections obtained due to the strong overlapping among lines decaying to different subshells.

For each of the incident energies mentioned in section 3, the refinement procedure was carried out following a very simple sequence, since the calibration parameters for the equipment used (zero and gain) have been repeatedly determined previously, which led to quite accurate initial guesses for them. After visual examination of the spectra, initial estimates were given for α_B . The refinement process was then completed, allowing these scaling factors to vary along with α_{L_i} , for which the initial values were set to 1. In order to corroborate the values obtained, the refinement procedure was repeated with different initial estimates for each of the parameters refined.

The experimental uncertainties associated with σ_x , and therefore with σ_{L_i} , are obtained by error propagation from (4) and (1). The contribution to these uncertainties due to the solid angle $\Delta\Omega$ is 6%, the number of incident electrons bears an error of 4%, the Ag film areal density uncertainty is 4%, and the detector efficiency is 3%. The uncertainties associated with ω_1 (28%), ω_2 (9%), and ω_3 (9%) have been estimated according to the scattering of data presented in the literature (see, e.g., [32]), whereas those associated with f_{12} (38%), f_{13} (30%), and f_{23} (35%) have been obtained from [33]. The statistical uncertainties related to characteristic peak determination depend on the intensity corresponding to the main peaks associated to each subshell and must be assessed as the square root of the number of counts recorded—in this case, subtracting the bremsstrahlung intensity under each peak, strongly influencing the smallest peaks. The average statistical uncertainties were 1% for the L_3 subshell, 3% for the L_2 subshell, and 16% for the L_1 subshell. In the present assessments, the final average errors are 38% for σ_{L_1} , 14% for σ_{L_2} , 19% for σ_{L_3} , and 12% for the total σ_x .

The ionization cross-sections determined depend on the choice for the parameters ω_i and f_{ij} . For this reason, the refinement procedure was performed twice, taking in one case as reference values for ω_i and Coster–Kronig transition probabilities those reported by Perkins *et al* [34], and in the other, those compiled by Campbell [33] (see table 1). Table 2 shows the results obtained for the two sets of parameters through this procedure; as expected, the resulting ionization cross-sections strongly depend on the reference parameters chosen.

The values determined by this procedure allow us to obtain the x-ray production cross-section for each incident

Table 2. Ionization cross-sections (in barns) obtained for the different L-subshells involving two sets of reference values: (a) Perkins *et al* [34]; (b) Campbell [33].

E_0 (keV)	σ_{L_1}		σ_{L_2}		σ_{L_3}	
	a	b	a	b	a	b
6	2640	2458	3172	3504	6276	7566
7	3112	2893	3518	3891	7222	8681
8	2792	2597	4037	4433	8098	9564
9	3275	3045	3817	4211	7805	9324
10	3276	3048	3990	4396	8260	9817
12	3316	3086	4229	4652	8101	9645
15	2876	2666	3852	4232	7841	9259
20	2698	2512	3420	3758	7100	8383
25	2067	1923	3026	3316	6588	7680

energy by means of (1) and (2). Table 3 displays the results produced for $\sigma_{L_i}^{\text{eff}}$ and σ_{L_x} , allowing comparison between the different sets chosen for ω_i and f_{ij} . It can be seen that despite the fact that each $\sigma_{L_i}^{\text{eff}}$ may change with the choice for these parameters, the final value obtained for σ_{L_x} remains unaltered; this makes sense, since σ_{L_x} represents the total contribution of all L emissions, and it is proportional to the number of counts detected in the whole L region of the spectrum.

Figures 5–7 display the values obtained for the ionization cross-sections for L_1 – L_3 subshells, respectively, as compared to the analytical models given by Campos *et al* [31] and Bote *et al* [35], both based on DWBA calculations. It is clear that the experimental determinations of the present work are always higher than the predicted values, regardless of which values are chosen for fluorescence yields and Coster–Kronig transition probabilities. It is worth mentioning that this comparison between DWBA calculations and experimental data for Ag has not been faced previously for this energy range.

Both sets of predictions ([31] and [35]) plotted in these figures essentially represent the same theoretical approach; the slight discrepancies observed between them (below 5%) may be attributed to the different parameterizations suggested. It is important to emphasize that the disagreement between theory and experiment observed in these plots has already been evidenced in [10], where comparisons have been carried out for experimental determinations in a higher energy range [36–38]; particularly for measurements performed at energies approaching those involved in this work, the discrepancies exhibited are similar to the present ones. Despite the experimental difficulties involved, the comparisons

Table 3. Effective ionization cross-sections $\sigma_{L_i}^{\text{eff}}$ (in barns) for the different L_i -subshells and total x-ray production cross-section σ_{L_X} , involving two sets of reference values: (a) Perkins *et al* [34]; (b) Campbell [33].

E_0 (keV)	$\sigma_{L_1}^{\text{eff}}$		$\sigma_{L_2}^{\text{eff}}$		$\sigma_{L_3}^{\text{eff}}$		σ_{L_X}	
	a	b	a	b	a	b	a	b
6	2640	2458	3415	3671	8578	9485	715	720
7	3112	2893	3804	4088	9900	10907	819	822
8	2792	2597	4294	4610	10642	11695	883	885
9	3275	3045	4118	4418	10642	11682	881	882
10	3276	3048	4292	4603	11125	12204	918	918
12	3316	3086	4535	4862	11032	12090	926	926
15	2876	2666	4117	4413	10413	11401	862	861
20	2698	2512	3669	3929	9482	10369	781	780
25	2067	1923	3217	3446	8477	9262	690	688

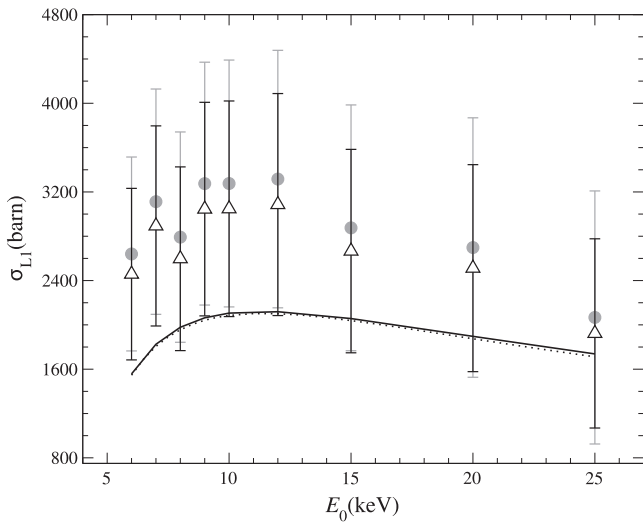


Figure 5. Ionization cross-section for the L_1 subshell obtained with two different sets of reference values, as compared to the DWBA values: ● Perkins *et al*; △ Campbell; — Campos *et al* [31]; Bote *et al* [35].

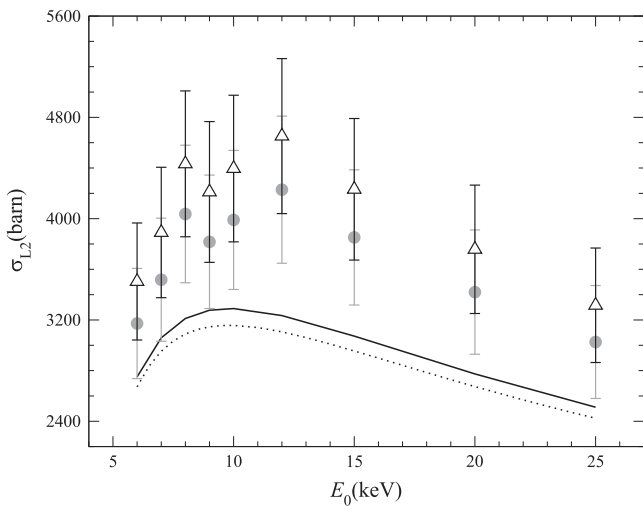


Figure 6. Ionization cross-section for the L_2 -subshell obtained with two different sets of reference values, as compared to the DWBA values: ● Perkins *et al*; △ Campbell; — Campos *et al* [31]; Bote *et al* [35].

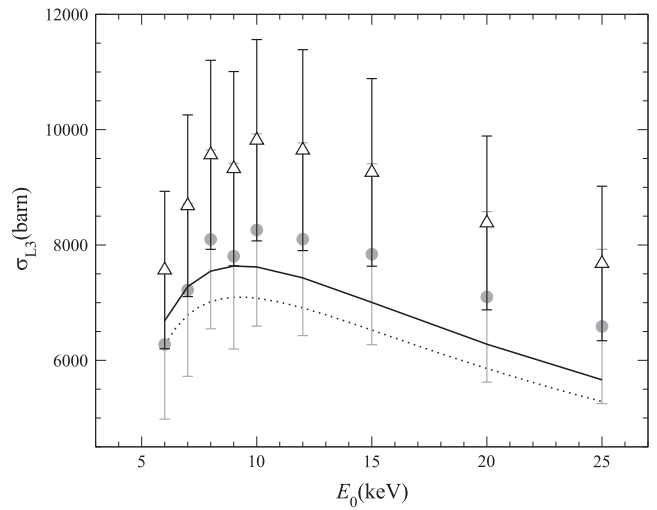


Figure 7. Ionization cross-section for the L_3 -subshell obtained with two different sets of reference values, as compared to the DWBA values: ● Perkins *et al*; △ Campbell; — Campos *et al* [31]; Bote *et al* [35].

displayed suggest that the DWBA approaches produce systematic underestimations in the energy range considered here.

The σ_{L_X} values obtained here are compared with those from the literature in figure 8. It can be seen that the present determinations are much higher than those reported by Wu *et al* [13]. In order to perform a comparison with the analytical prediction for σ_{L_i} given by Campos *et al* it is necessary to choose a set of ω_i . The predicted x-ray production cross-sections lie between the present experimental data and those from [13]. The discrepancies between both sets of experimental data may be due to several reasons. First, the energy resolutions are different for the spectrometers involved, since the better resolution used in this work allows us to discriminate a greater number of peaks associated with decays to each subshell. On the other hand, the present choice of a carbon substrate allows us to reduce both the backscattered electron contribution to the ionizations generated in the Ag film and the bremsstrahlung emission, as compared with an aluminum substrate like that used in [13]. The inaccuracies in

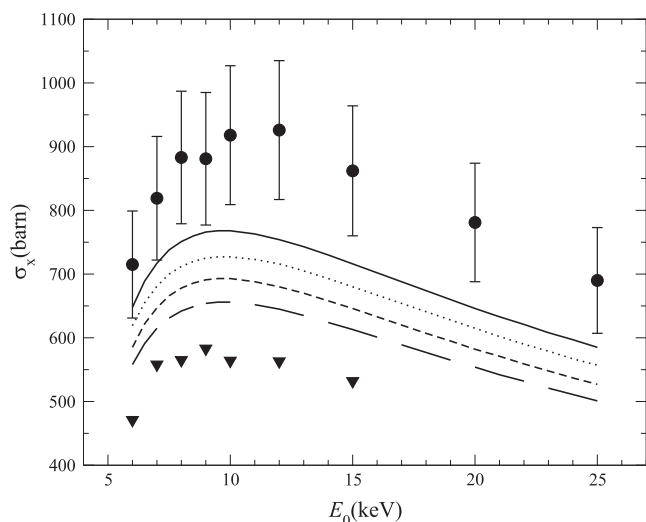


Figure 8. Total x-ray production cross-sections for the L-shell, as compared with the Wu *et al* experimental data [13] and the DWBA σ_{Lx} of Campos *et al* [31] and Bote *et al* [35], calculated with the two sets of reference values: ● This work; — Campos with Perkins *et al*; - - - Campos with Campbell; ····· Bote with Perkins *et al*; — · — Bote with Campbell; ▼ Wu *et al*.

the prediction of these contributions in the data presented in this work are therefore less important.

5. Conclusions

The ionization cross-sections for each L-subshell and the total L-shell x-ray production cross-section for Ag have been experimentally determined for incident electron energies between 6–25 keV. The values obtained for σ_{L_i} represent an important contribution since, to the best of the authors' knowledge, this is the first time these magnitudes are reported in the literature for this energy range.

The results obtained have been compared with analytical predictions based on DWBA calculations [31, 35], a similar trend being observed, although the predicted values underestimate the experimental determinations of the present work. In the case of the total L-shell x-ray production cross-section, the present results have also been compared with the only previous experimental data found [13]; the discrepancies found may be originated in the different experimental settings for both investigations. Obviously, it is necessary to count with additional experimental determinations in order to be conclusive regarding the disagreement between the different data sets.

An important limitation for the data processing is the uncertain reliability for the ω_i and f_{ij} parameters. Since it is impossible to avoid the use of these parameters, work must be done to develop methodologies which allow us to determine them with better accuracy.

Inasmuch as bulk samples offer counting rates higher than those from thin films, an alternative procedure has been proposed [18, 19]. The use of this approach allows us to avoid the experimental difficulties in the fabrication of thin targets

as well as in the determination of their thickness. In the future, work will be done with this model in order to improve the x-ray attenuation corrections and the electron backscattering losses.

Acknowledgements

The authors are grateful for financial support from the Coordenação de Aperfeiçoamento de Pessoal de Nível Superior-CAPES (Brazil) and the Secretaría de Políticas Universitarias del Ministerio de Educación-SPU (Argentina).

References

- [1] Friel J J and Lyman C E 2006 Tutorial review: X-ray mapping in electron-beam instruments *Microsc. Microanal.* **12** 2–25
- [2] Egerton R F, Qian H and Malac M 2006 Improving the energy resolution of x-ray and electron energy-loss spectra. *Micron* **37** 310–15
- [3] Egerton R F 2009 Electron energy-loss spectroscopy in the TEM *Rep. Prog. Phys.* **72** 016502
- [4] Limandri S, Bonetto R, Galván Josa V, Carreras A and Trincavelli J 2012 Standardless quantification by parameter optimization in electron probe microanalysis *Spectrochim. Acta B* **77** 44–51
- [5] Khare S P, Saksena V and Wadehra J M 1993 K-shell ionization of atoms by electron and positron impact *Phys. Rev. A* **48** 1209–13
- [6] Rez P 2002 Accurate cross sections for microanalysis *J. Res. Natl. Inst. Stand. Technol.* **107** 487–95
- [7] Segui S, Dingfelder M and Salvat F 2003 Distorted-wave calculation of cross sections for inner shell ionization by electron and positron impact *Phys. Rev. A* **67** 062710
- [8] Bote D and Salvat F 2008 Calculations of inner-shell ionization by electron impact with the distorted-wave and plane-wave Born approximations *Phys. Rev. A* **77** 042701
- [9] Fernández-Varea J M, Segui S and Dingfelder M 2011 L_{α} , L_{β} , and L_{γ} x-ray production cross sections of Hf, Ta, W, Re, Os, Au, Pb, and Bi by electron impact: Comparison of distorted-wave calculations with experiment *Phys. Rev. A* **83** 022702
- [10] Llovet X, Powell C J, Salvat F and Jablonski A 2014 Cross sections for inner-shell ionization by electron impact *J. Phys. Chem. Ref. Data* **43** 013102
- [11] Kim Y and Desclaux J P 2002 Binary-encounter-dipole model for electron-impact ionization *Phys. Rev. A* **50** 3954–67
- [12] Kim Y and Desclaux J P 2002 Ionization of carbon, nitrogen, and oxygen by electron impact *Phys. Rev. A* **66** 012708
- [13] Llovet X, Merlet C and Salvat F 2002 Measurements of L-shell x-ray production cross-sections of Au and Ag by low energy electron impact. *J. Phys. B: At. Mol. Opt. Phys.* **35** 973–82
- [14] Llovet X, Merlet C and Salvat F 2002 Measurements of absolute cross sections for K-shell ionization of Fe and Mn by electron impact. *J. Phys B: At. Mol. Opt. Phys.* **35** 973–82
- [15] Moy A, Merlet C, Llovet X and Dugne O 2013 Measurements of absolute L- and M-subshell x-ray production cross sections of Pb by electron impact. *J. Phys B: At. Mol. Opt. Phys.* **46** 115202
- [16] Zhengming L, Changhuan T, Zhu A, Fuqing H, Xiufeng P and Xianguan L 2001 Selenium and yttrium K-shell ionization cross-sections by electron impact *Phys. Rev. A* **63** 034702
- [17] Limandri S, Vasconcellos M A Z, Hinrichs R and Trincavelli J 2012 Experimental determination of cross sections for K-

- shell ionization by electron impact for C, O, Al, Si, and Ti *Phys. Rev. A* **84** 042701
- [18] An Z, Wu Y, Liu M T, Duan Y M and Tang C H 2006 Thick-target method in the measurement of inner-shell ionization cross-sections by low-energy electron impact *Nucl. Inst. Meth. B* **2046** 281–87
- [19] An Z and Hou Q 2008 Inverse problem in the thick-target method of measurements of inner-shell ionization cross sections by electron or positron impact *Phys. Rev. A* **77** 042702
- [20] Bambynek W, Crasemann B, Fink R W, Freund H-U, Mark H, Swift C D, Price R E and Venugopala Rao P 1972 X-ray fluorescence yields, Auger, and Coster–Kronig Transition Probabilities. *Rev. Mod. Phys.* **44** 716–813
- [21] Merlet C, Llovet X and Salvat F 2008 Near-threshold absolute M-shell x-ray production cross sections of Au and Bi by electron impact *Phys. Rev. A* **78** 022704
- [22] Wu Y, An Z, Duan Y M, Liu M T and Wu J 2011 K-shell ionization cross sections of Cl and L_{α} , L_{β} x-ray production cross sections of Ba by 6–30 keV electron impact *Nucl. Inst. Meth. B* **269** 117–21
- [23] Bonetto R, Castellano G and Trincavelli J 2001 Optimization of parameters in electron probe microanalysis *X-Ray Spectrom.* **30** 313–19
- [24] Limandri S, Trincavelli J, Bonetto R and Carreras A 2008 Structure of the Pb, Bi, Th, and U M x-ray spectra *Phys. Rev. A* **78** 022518
- [25] Mayer M 1997 *SIMNRA User Guide Technical Report IPP 9/113 Max Planck Institut für Plasmaphysik* (Germany: Garching)
- [26] Rodríguez T, Carreras A, Sepúlveda A, Bertol A P L, Castellano G, Vasconcellos M A Z, Hinrichs R and Trincavelli J 2013 Structure of the x-ray emission L spectra for elements with atomic number between 26 and 52 by electron incidence *13th Int. Conf. on PIXE*
- [27] Limandri S, Carreras A, Bonetto R and Trincavelli J 2010 K_{β} satellite and forbidden transitions in elements with $12 \leq Z \leq 30$ induced by electron impact *Phys. Rev. A* **81** 1–10
- [28] Trincavelli J and Castellano G 2008 The prediction of thick target electron bremsstrahlung spectra in the 0.25–50 keV range *Spectrochim. Acta B* **63** 1–8
- [29] Visňovezky C, Limandri S, Canafoglia M E, Bonetto R and Trincavelli J 2007 Asymmetry of characteristic x-ray peaks obtained by a Si(Li) detector *Spectrochim. Acta B* **62** 492–98
- [30] Salvat F, Fernández-Varea J M and Sempau J 2011 PENELOPE 2011—A code system for Monte Carlo simulation of electron and photon transport (Paris: Issy-les-Moulineaux) OECD/NEA Data Bank
- [31] Campos C S, Vasconcellos M A Z, Trincavelli J C and Segui S 2007 Analytical expression for K- and L-shell cross sections of neutral atoms near ionization threshold by electron impact *J. Phys. B: At. Mol. Opt. Phys* **40** 3835–41
- [32] Zschorneck G 2007 *Handbook of X-Ray Data* (Berlin: Springer)
- [33] Campbell J L 2003 Fluorescence yields and Coster–Kronig probabilities for the atomic L subshells *At. Data Nucl. Data Tables* **85** 291–315
- [34] Perkins S T, Cullen D E, Chen M H, Hubbell J H, Rathkopf J and Scofield J H 1991 *Lawrence Livermore National Laboratory, Livermore Report UCRL-50400* 30
- [35] Bote D, Salvat F, Jablonski A and Powell C 2009 Cross sections for ionization of K, L and M shells of atoms by impact of electrons and positrons with energies up to 1 GeV: Analytical formulas *At. Data Nucl. Data Tables* **95** 871–909
- [36] Hoffmann D H H, Brendel C, Genz H, Löw W, Müller S and Richter A 1979 Inner-shell ionization by relativistic electron impact *Z. Phys. A* **298** 187–201
- [37] Genz H, Brendel C, Eschwey P, Kuhn U, Löw W, Richter A, Seserko P and Sauerwein R 1982 Search for the density effect in inner-shell ionization by ultra relativistic electron impact *Z. Phys. A* **305** 9–19
- [38] Reusch S, Genz H, Löw W and Richter A 1986 A method to determine L-subshell ionization cross sections for medium and heavy elements *Z. Phys. D* **3** 379–89